03,09

Unusual defects in CVD diamond

© S.Yu. Martyushov[1], I.L. Shul'pina[2], A.A. Lomov[3], S.N. Polyakov[1]

[1] Technological Institute for Superhard and Novel Carbon Materials, Moscow, Russia
[2] Ioffe Institute, St. Petersburg, Russia
[3] Valiev Institute of Physics and Technology, Russian Academy of Sciences, Moscow, Russia

E-mail: mart@tisnum.ru

Received July 17, 2023
Revised August 4, 2023
Accepted August 5, 2023

Structural defects of a diamond grown homoepitaxially by chemical vapor deposition (CVD) on a single-crystal substrate of a Ib diamond obtained by the high-pressure high-temperature method (HPHT) were studied using the methods of X-ray diffraction imaging (projection and section X-ray topography) and high-resolution (double-crystal) X-ray diffractometry. It is shown that there are no HPHT substrate defects in CVD diamond, but new ones are present — stacking faults of an unusual type and structure, which coexist with highly perfect crystal regions suitable for manufacturing elements of X-ray optics. For the first time, macrodefects were discovered, which were previously observed only in dislocation-free silicon single crystals.

Keywords: HPHT diamond, synthetic diamond, structural defects, dislocations, stacking faults, X-ray diffraction imaging, section and projection topography, high-resolution X-ray diffractometry.

DOI: 10.61011/PSS.2023.11.57311.154

1. Introduction

Due to its unique properties, diamond is the most suitable material for the use in extreme conditions in various applications [1–5]. In this context, structure–sensitive properties (electrical, optical, mechanical, etc.) of diamond are the subject of permanent research [6]. Most of the properties of diamond single crystal depend on its real structure and are determined by the type, quantity, and distribution of growth, impurity, intrinsic and thermal defects contained in it. Therefore, special requirements are imposed on the perfection of the crystalline structure of diamond and the content of impurities. This greatly limits or makes it impossible to use natural diamond single crystals due to the imperfection of their structure.

The synthetic diamonds are grown under conditions of high pressure and high temperature (HPHT) or by plasma chemical deposition (CVD and its modifications — PECVD, MPACVD, etc.) [6,7]. Despite the enormous progress in the technology of growing perfect diamond crystals [8–12] the problem of producing defect-free single crystals has not been completely solved. Therefore, the improvement of existing and development of new technological approaches to solve the problem of growing perfect diamond single crystals is under the close attention of researchers. A special role is given to the study of large growth structural defects determined by the growth mechanism and depending on technological conditions.

The HPHT method makes it possible to grow synthetic diamonds in the shape of a tetrahedron with dimensions up to $10 \times 10 \times 6\,\text{mm}^3$ with residual stresses of the order of 0.1 MPa [9]. Dislocation-free single-crystal wafers with a surface roughness of 0.4 nm can be made from them [13]. However, a feature of HPHT growth conditions is the possible introduction of uncontrolled inclusions of metals (Fe, Ni, Al) [14] used as catalysts into diamond single crystals.

Depending on the growth conditions, dislocations, stacking faults, and inclusions are formed in diamond single crystals, some of which are associated with interstitial impurity atoms. Depending on the type and concentration of the impurity, diamond crystals are divided into type I and II with subgroups *a* and *b* [15]. The main natural impurity is nitrogen, and the main doping impurity is boron. Natural diamond crystals are classified as type I*a*. Their main impurity is nitrogen with a concentration of $C_N > 5-100$ ppm. A diamond grown by the HPHT method with a large amount of nitrogen and doped with boron is classified as group I*b*. The CVD technology allows controlling the nitrogen content in the crystal in the process of growth and reducing its concentration down to 100 ppb [10]. The decrease in the impurity concentration in CVD diamond single crystals should lead, in principle, to a decrease in the concentration of large structural defects.

For the growth of diamond films and single crystals, single-crystal HPHT diamond films and single crystals, single-crystal HPHT diamond substrates with orientation of (001) and a thickness of ~ 1 mm are usually used [7,16]. Despite the homoepitaxial growth, standard grown diamond-like films are very defective. They not only

inherit structural defects from the substrate: the boundaries of growth sectors and growth bands, and the boundaries of dislocations in the sectors, stacking faults, impurity precipitation and inclusions, but due to the relaxation of stresses at the interface with the substrate, they also acquire their own defects.

It is known that diamond is characterized by a sectorial growth nature [17,18]. Due to the sectorial nature of the growth of diamond single crystal, a non-uniform distribution of impurities occurs. An increased concentration of impurities, mainly nitrogen, at the boundaries of growth sectors causes deformation of the crystal lattice. Inside the sectors, the lattice deformation is less and manifests in the form of growth bands on topograms. Excess nitrogen results in an increase in the crystal lattice constant. The nitrogen concentration in growth sectors decreases in $(111) > (100) > (113) > (110)$ directions of growth sector orientation. The number of defects decreases in the same direction.

The most effective studies of dislocations in diamond crystals have been carried out using X-ray topography, optics, and cathodoluminescence methods. Currently, the types of almost all dislocations observed in HPHT crystal types II*a* and I*b* [19,20] have been determined. It has been shown that up to 84% of dislocations in crystals of type II*a* are directed along $\langle 101 \rangle$, and up to 71% of dislocations in crystals of type I*b* are directed along $\langle 11\underline{2} \rangle$. Most dislocations have Burgers vectors [110] and [1$\bar{1}$0] with a zero component along the *c*-axis of the cubic crystal, being edge dislocations (47 and 65% for crystal types II*a* and I*b*, respectively). In addition to them, additional 60 and 73-degree screw dislocations are observed in type II*a*, and 30, 35, and 73-degree dislocations are observed in type I*a*. In [10,21], it is shown that in CVD crystals homoepitaxially grown on HPHT crystals as substrates, dislocation bundles or clusters are observed. Dislocation clusters originate from isolated points on or near the top surface of the substrates. As a rule, clusters contain several edge-type dislocations. It is clear that as a result, there will be more dislocations in CVD-crystals than in HPHT-crystal-substrates.

Damage of the surface of the substrate is mainly associated with 45-degree dislocations, the Burgers vector component of which is parallel to the polishing direction. Dislocations in CVD-crystals are usually observed in bundles rather than individually. Networks of dislocations typical for the heteroepitaxy of semiconductor structures are not observed in CVD-diamonds [22]. At the same time, the formation of dislocation misfit half-loops is possible at the interface with the substrate.

In addition to dislocations, stacking faults are observed in CVD-crystals. They are of planar type and lie in the $\{111\}$ planes. These defects can be large in area, reaching several square millimeters in large crystals. Their number increases in the direction from the center of crystals to the side facets. Planar stacking faults in substrates can be sources of dislocations in CVD-crystals when they cross the interface. In [24], it was determined that in most cases CVD-crystals exhibit stacking faults of intrinsic type.

Due to the fact that stress relaxation in the bulk of the crystal is determined by the formation of various structural defects in them, progress in the technology of growing perfect diamonds is impossible without studying their real structure. Structural defects in diamond crystals have been studied for a long time [25] and using different methods [15,25,26]. However, as research shows, structural defects in diamond have not been fully studied and new ones are being discovered [27].

Until now, it was believed that single-crystal diamond films homoepitaxially grown by plasma-enhanced chemical vapor deposition (PECVD) were significantly inferior in structural perfection to HPHT diamond crystals. However, it has been shown that the use of nitrogen-containing single-crystal HPHT I*b* substrates makes it possible to grow large and highly perfect CVD-diamond single crystals with a size of $10 \times 10 \times 1.7\,\text{mm}^3$. The perfection of the crystal lattice of CVD-diamonds turned out to be comparable to that of HPHT II*a* diamond single crystals [9]. In particular, the area of the plate with a size of at least $3 \times 3 \times 1.5\,\text{mm}^3$ turned out to be a highly perfect single crystal and, with the exception of point defects, did contain neither growth-related structural defects nor structural defects inherited from the substrate. At the same time, in other parts of the CVD-plate there were defects of an unusual type, which had not previously been observed in diamond crystals. These defects are discussed in this study.

The methods of X-ray topography and high-resolution diffractometry are traditionally used to diagnose the structural perfection of the lattice and visualize extended defects in the bulk of the crystal [30–34]. Due to the low X-ray absorption coefficient for diamond, from $\mu = 0.48\,\text{cm}^{-1}$ to $\mu = 12.46\,\text{cm}^{-1}$ in the wavelength range from 0.056 nm ($\text{Ag}K_\alpha$) to 0.154 nm ($\text{Cu}K_\alpha$), Bragg and Laue geometries can be used to study crystals with a thickness of up to a few mm. In this study, X-ray methods are used for a comprehensive investigation of known and unusual defects observed for the first time in CVD-diamonds. We believe that this will allow for better understanding of the mechanism of stress relaxation in the diamond.

2. Experiment procedure

Structural defects were investigated in single crystals: the HPHT I*b* (100) substrate and CVD (100) thick plate with dimensions of $10 \times 10 \times 1.7\,\text{mm}^3$. It should be noted that the CVD crystal in the form of a thick plate was separated from the seed HPHT crystal substrate using a laser.

To study the real structure of crystals, methods of X-ray diffraction topography and high-resolution X-ray diffractometry were used [30,31]. Topograms were recorded on a Rigaku XRT−100 CCM setup (Japan) with a rotating anode with a power of 18 kW. $\text{Ag}K_\alpha$ and $\text{Mo}K_\alpha$ radiation was used at a voltage of 50 kV and a current of 100 mA,

with a reflection of 220. To obtain Lang projection topograms, size of the slit at the outlet of the vacuum path was 0.5 mm, and to obtain sectional topograms, it was 0.01 mm. Images were recorded on Fujifilm ix# 50 film. In addition to projection topograms, a series of sectional topograms were taken with movement of the plate along the diffraction vector. The exposure time for one topogram was 2 h.

Projection and sectional methods of X-ray topography (XRT) were used. The sectional XRT method is promising for diamond crystals due to the low absorption of X-rays. Moreover, it is 20 times more sensitive than the Lang projection method with respect to weak disturbances in the crystal lattice of single crystals [32,33], because it is based on interference phenomena in the crystal. Its important feature is the presence of interference fringes or Kato fringes, which are observed only for crystals whose lattice disturbances do not exceed $\Delta d/d = 10^{-6}$. The absence of Kato fringes on sectional topograms corresponds to the static Debye–Waller factor of $L > 0.02$ [34].

The factor L is used in X-ray diffractometry as a measure of integral disturbances of the average crystal lattice. The use of the sectional method allows obtaining additional information about the distribution of defects over the thickness of the samples, because the width of the sectional topogram reflects the distribution of defects throughout the thickness of the sample.

Double-crystal diffraction reflection curves (DRC) were recorded using CuK_β radiation in the Bragg geometry according to a dispersion-free scheme $(n, -n)$ on a TRS three-crystal X-ray spectrometer (Special Design Bureau of the Institute for Crystallography of the Academy of Sciences). The monochromator crystal was a HPHT flat diamond with a (100) surface orientation [35]. Diffraction reflection curves 004 (Bragg angle $\theta = 51.32°$) were recorded with a step of 0.3 arcsec from different sections of the sample relative to the edge of the sample at $x = 0$ (Figure 1) with a step of 0.5 mm.

3. Experimental results

3.1. Structural defects of the HPHT substrate

The HPHT temperature-gradient method allows growing single crystals with maximum sizes of $10 \times 10 \times 10\,\text{mm}^3$. The method makes it possible to grow single crystals containing few defects. Currently, it has no alternative precisely from this point of view.

The $10 \times 10 \times 0.7\,\text{mm}^3$ substrate was fabricated from a type I*b* crystal grown using the HPHT method. The substrate contained few dislocations and stacking faults. The most pronounced defects in it were the boundaries of growth sectors, Figure 1, *a*. These are the places where everything not included in the lattice is driven back aside during crystal growth, primarily impurities and associated microdefects. In growth sectors, growth bands with an increased impurity concentration, microdefects, and individual dislocations connecting some bands were observed. Planar stacking faults were also present, appearing on topograms as areas of solid halftone contrast. There are more of them at the side facets of the crystal than in the center. Thus, the structural perfection of our substrate was typical for type I*b* HPHT crystals. A distinctive feature of the substrate structure was the presence of an inclusion with a strong stress field around it. It was so strong that it was inherited by the CVD crystal layer growing on the substrate and even enhanced in it, Figure 1, *b*.

3.2. Structural defects in the CVD-diamond

Let us consider separately the types of defects observed in the plate under study: dislocations, stacking faults, and macrodefects.

Dislocations. It is noteworthy that the plate lacks inheritance of substrate dislocations, Figure 1, *b*. In the plate, the presence of dislocations near the interface and in places of strong stresses inherited from the substrate would be expected: the region around the inclusion and the region that is a projection of the strongly pronounced boundary of the growth sectors (*1* and *3* in Figure 1, *a*). However, despite the strong stresses around the inclusion, dislocations are not detected there. As for the band in the projection of the boundary of growth sectors in the substrate, it is very similar to the dislocation slip band, but this is not the case. The following features of the band image can be distinguished, Figure 1, *b*: 1) the background of the band image is continuous and non-uniform, which is indicative of remaining stresses that have not been completely relaxed due to the formation of defects; 2) defects in the band are linear-shaped and grouped into packs. Images of defects are pairs of lines at an angle of about 40° to each other with a common point in the form of a spot on one boundary of the band, Figure 2, *a*. They are similar to dislocations, however, in our opinion, they represent groups of special stacking faults (SF), which are observed in the plate and in a single form outside the band in the upper right corner in Figure 1, *b*. However, single defects have much weaker contrast than their counterparts in the band. This is explained by the peculiarity of X-ray topographic images of defects — in the stress region, the contrast of defects increases. In a single form, these SFs are located in the region of the plate where there are no stresses and the contrast of defects is very weak. In terms of type of image, these defects are similar to stacking faults in homoepitaxial layers of SiC-6H crystals, which structure was determined in [36]. This required the use of three main XRT methods: Lang's method, method of anomalous X-ray transmission (AXRT), and method of Bragg reflection. The images of these defects were highly dependent on the reflections used to record the topograms. In [36], the rule was defined to establish the reflections for SiC-6H crystals where the most characteristic feature of the image of these defects is observed, by which their confident identification is made, i. e. the continuous contrast between the boundaries.

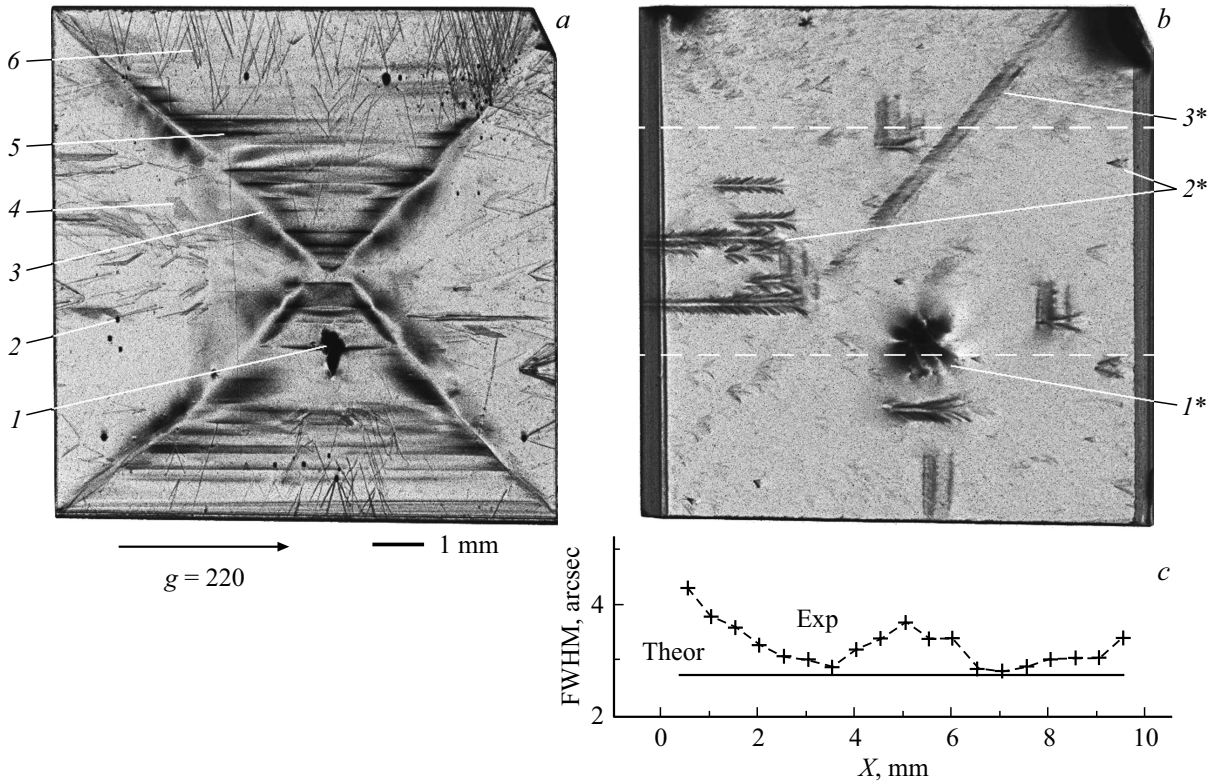

Figure 1. X-ray topograms of diamond single crystals (a, b), DRC half-width of reflection 004 depending on the location of illumination X on the surface of the plate (c). Lang method, reflection 220, Ag$K_{\alpha 1}$ radiation, direction of the diffraction vector is shown with an arrow. DRC: reflection 004, CuK_{β} radiation. Numbers in (a) indicate: *1* — macroinclusion, *2* — small inclusions, *3* — boundaries of growth sectors, *4* — stacking faults, *5* — growth bands, *6* — individual dislocations. In (b): *1** — inheritance of stresses from macroinclusion, *2** — bulk stacking faults in clusters and individual ones, *3** — band with stacking faults in the projection of the boundaries of growth sectors in the substrate. White dashed lines show the area where DRC is recorded by an X-ray beam with a cross section of 4 mm in height and a width of 150 μm (c).

The boundaries of these SFs were partial dislocations, and the common point was a rosette of microstresses from a sessile stair-rod dislocation, which are manifested in the topograms taken by the AXRT method. Conventionally, we call these type 1 SFs. Their typical images in the diamond plate are shown in Figure 2, *a*.

The similarity of defects in the epitaxial layers of diamond and silicon carbide crystals is not accidental. The elastic properties of these crystals are determined by the high Debye temperature and the relatively low epitaxy temperature. We will discuss it later.

Thus, dislocations are not the main type of defects in the CVD-crystal. They are not inherited from the substrate and are not formed during crystal growth. The CVD crystal has inherited from the substrate only regions of high stress, where partial stress relaxation is possible with the formation of new defects, however, not dislocations, but SFs.

Stacking faults. The main defects in the wafer are SFs, but of a different type than those in the substrate. They are not planar, but bulk defects, sometimes built into each other, combined into packs. And type 1 SFs are not the only type of such defects in the diamond. An example of another type of defects is the cluster at the left edge

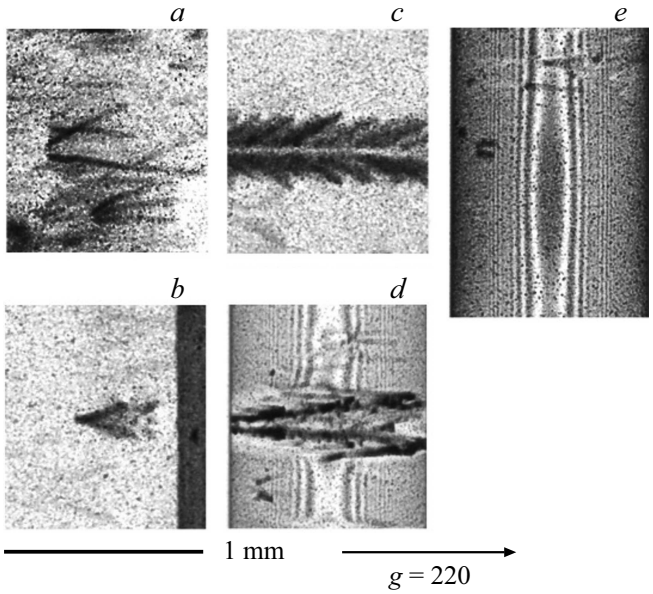

Figure 2. Fragments of topograms of the CVD wafer. Projection images of SF type 1 (a, b), projection (c) and sectional (d) image of SF type 2, image of a macrodefect on the sectional topogram (e).

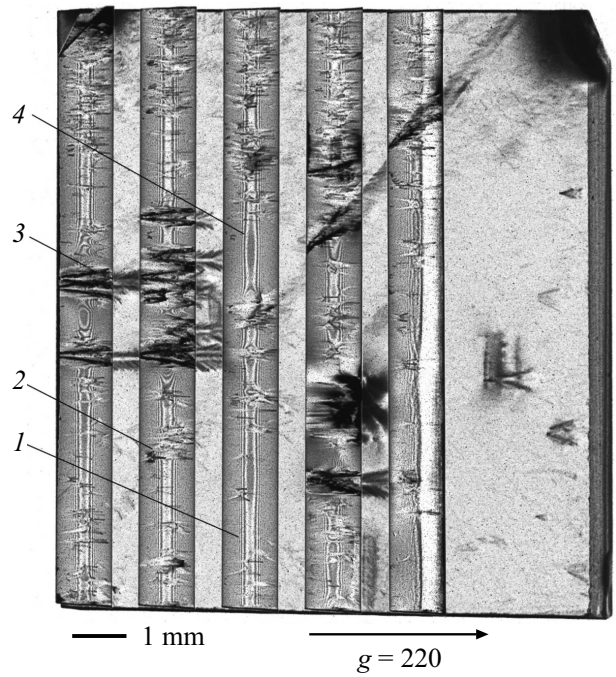

Figure 3. A series of 5 consecutive sectional topograms superimposed on the projection topogram of the CVD-crystal. The step between topograms is 2 mm. Recording conditions are as follows: reflection 220, Ag$K_{\alpha 1}$ radiation, direction of the diffraction vector is shown by arrow, slit size is 10 μm, recording time of each section is 120 min. *1*) area with almost undistorted interference fringes, *2*) type 1 SF, *3*) type 2 SF, *4*) macrodefect.

of the wafer (*2** Figure 1, *b*). They are also present in the individual form. In the topogram *1*, *b* and its fragment in Figure 2, *c*, they are represented by rectangles of solid contrast of a relatively large size with borders in the form of fringes (or herringbones). Sectional topograms show that their structure is even more complex: when deepening into the thickness of the wafer, they have one end bifurcated, Figure 2, *d*. Sectional images of these defects show that they are not planar, but bulk (three-dimensional) defects with a complex structure and are presented in two orientations in the wafer with an elongated facet along one of two {110} directions. Conventionally, we call these SFs type 2. Defects of this type have previously been observed neither in diamond nor in other crystals. The origin of these defects is still unclear. A detailed analysis of the structure of this type of defects has yet to be done.

Macrodefects. Figure 3 shows projection topogram of a part of the wafer with several sectional topograms superimposed on it, taken in the same reflection with shifts of the wafer in the direction of the diffraction vector. This technique allows obtaining additional information about defects.

When examining sectional topograms, in some of them areas can be noted with the changes in the shape and periodicity of interference fringes, Figure 3.

Their size, determined in the anti-Bragg direction as the distance between the points where the shape and periodicity of the interference fringes changes, can be as large as 2 mm. At the same time, no defects are observed on the projection topograms in these places of the wafer. This means that defects in these areas of sectional topograms do not create a direct (kinematic) image on projection topograms, because the crystal lattice stresses associated with them are very weak. They can only be detected by extremely sensitive sectional X-ray topography. Such defects were first discovered in dislocation-free silicon single crystals and described in [33], where they were called macrodefects.

They were observed in dislocation-free silicon crystals grown using the Czochralski method. The oxygen content was $7 \cdot 10^{17}$ cm^{-3}. The crystals were subjected to multi-stage heat treatment in a neutral atmosphere. Macrodefects up to 1 mm in size appeared only on sectional topograms as a perturbation of the dynamic fringe pattern of a perfect crystal and did not create a kinematic image. It should be noted that interference fringe interruptions were observed at the ends above and below these sections (see Figure 1 and 2,*c* in [33]). The distance between these interference fringe upsets was 890 and 840 μm. The authors of [33] concluded that these defects were bulk macroregions where diffraction characteristics of the crystal (the real part of the polarizability or the refraction index) changed, and these changes were extremely insignificant. The above-described defects were observed only by the sectional XRT method and only in dislocation-free silicon crystals. The authors of the article considered the most likely cause of the observed defect formation to be the not uniform distribution of dispersed oxygen-containing precipitates in the bulk of the studied crystals, caused by the not uniform distribution of oxygen in the initial single crystals

Later, in [34], using the sectional XRT method, a macrodefect was also discovered in a dislocation-free silicon crystal doped with phosphorus to a concentration of $1.1 \cdot 10^{20}$ cm^{-3} in the *as-grown* state, that did not create a kinematic image. It was significantly smaller in terms of its size (250 μm), and the stress field associated with it was weaker. In the sectional topogram, there were no interruptions of the interference fringes at the ends of the image of this defect, but only their smooth displacement and distortion (curvature). Its image is shown in [34 and 32]

In the images of macrodefects in the diamond wafer, Figure 2 and 3, also there is no interference fringe upset and only a smooth curvature is observed. The stress field associated with them is weaker and closer to the macrodefect in [34]. Due to the fact that macrodefects with a weak stress field were observed only in dislocation-free silicon crystals, their detection in a diamond wafer confirms its high structural perfection and the absence of dislocations.

3.3. Assessment of the structural perfection of the CVD-diamond wafer

The structural perfection of the CVD-diamond wafer near-surface layer was assessed on the basis of the numerical values of the parameters of double-crystal DRC curves. A RC curve is a convolution of the sample's own (Darwin) reflection curve and the curve of reflection from the monochromator crystal. In the case, when the quality of the monochromator crystal is unknown, uncertainty arises in assessing the structural perfection of the crystal being characterized. It is worth noting that due to the low polarizability of diamond, and, as a consequence, an angular width of its own reflection curve of an order of a few seconds, it is more convenient to take a diamond monochromator crystal with known parameters to record the RC. In this study, a dislocation-free HPHT-diamond wafer with a surface orientation of (001) [35] was used as a monochromator crystal to record experimental RC curves. The cross section of the incident X-ray beam on the sample was equal to 0.1×4 mm. Figure 4, *b* shows the experimentally obtained double-crystal RC from the defect-free region of the CVD crystal, as well as the calculated diffraction reflection curves for ideal crystals [36]. The calculation was performed both for the own reflection curve of for the ideal diamond crystal and taking into account the convolution with the HPHT monochromator crystal.

It can be seen that the experimental RC (*1*) is almost no different from the theoretical RC (*4*) calculated for highly perfect crystals of the sample and monochromator. The observed slight difference in the behavior of the curve tails at $2-4$ arcsec can be associated both with large defects caught in the 0.15×4 mm field of surface illumination by the X-ray beam, and with the „tails" of the instrumental function that distorts the wave front on the sample. The type of instrumental function is determined by the monochromator crystal, collimator slits, and other experimental conditions. The main parameters of the experimental curve, i.e. reflectance $P_R = 85\%$ and half-width $\omega = 2.7-2.8$ arcsec are close to theoretical values. Based on the dynamic theory of scattering [37], thickness of the surface layer of the wafer, which contributes to scattering, was estimated as $20-30\,\mu$m. Thus, the high structural perfection of the surface layer of the CVD-diamond wafer was confirmed. In this experiment, we can say that the single-crystal diamond grown by the PECVD method is not inferior in perfection to the HPHT diamond [35].

Structural perfection in the bulk crystal was assessed by the proportion of regions with well-defined interference fringes in a series of sectional topograms superimposed on the projection topogram of the entire diamond wafer (not shown). The deformation of crystal lattice in these regions was less than 10^{-6}. As a result, it was concluded that in the studied wafer there were several fairly large regions without defects that could upset the interference fringes.

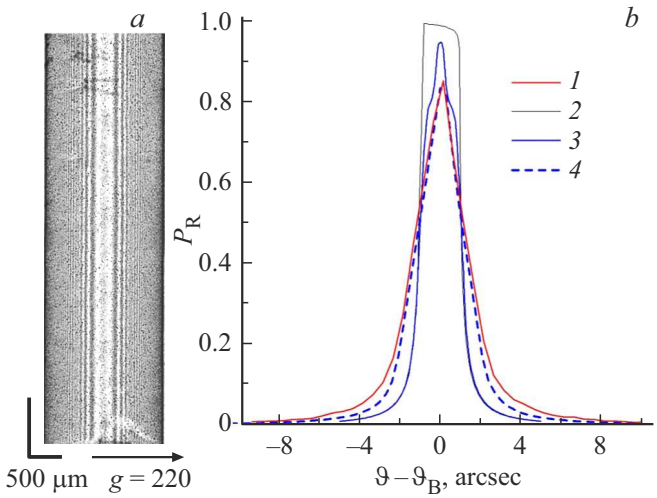

Figure 4. Fragment of the sectional topogram of a defect-free region of the CVD diamond, Ag$K_{\alpha 1}$ radiation, reflection 220 (*a*). Experimental RC (*1*) from this region and theoretical intrinsic (Darwin) curves from a highly perfect diamond crystal for polarization C_σ (*2*) and $C_\sigma + C_\pi$ (*3*), theoretical RC (*4*) taking into account convolution with a diamond monochromator crystal. reflection 004, CuK_β radiation (*b*).

Plotting the curve of RC half-width as a function of position in the crystal on the projection topogram, Figure 1, *b*, made it possible to obtain additional information by determining which defects and at what position along the crystal thickness affected the RC broadening to the greatest extent. As expected, these turned out to be the stresses inherited from the substrate around the inclusion, as well as large bulk type 2 SFs. It is noticeable that large bulk type 2 SFs have this effect when they are located in the near-surface layer of the crystal from which the RC were recorded. When they are deepened along the wafer thickness, as shown by their sectional image (see the left edge of the curve and topogram in Figure 1, *b*), this effect is greatly reduced. Single type 1 SFs, as well as macrodefects, have little effect on the broadening of the RC.

4. Discussion of results

Stress relaxation in diamond at the interface of substrate–film or substrate–thick layer during homoepitaxy can occur in different ways. It was noted in [22], that when growing CVD-diamond films on HPHT substrates, a growth regime is possible where stress relaxation occurs differently than that observed in silicon, germanium, and other crystals according to the classical scheme. It can be carried out through bending of thin films. In the process of growing of our diamond single plate, the introduction of an intermediate layer with a thickness of $100\,\mu$m [28,29] had a certain effect on the stress relaxation. This layer created a barrier for substrate defects that they could not overcome. Only areas of strong stress around the inclusion and at

the boundaries of growth sectors were inherited, and new defects arose in the plate and they became stacking faults the shape and structure have not been observed before.

Type 1 SFs are similar in the nature of their images on topograms to defects in homoepitaxial layers of 6H-SiC single crystals, whose structure was determined in [38]. The shape of these defects in 6H-SiC crystals is close to a tetrahedron.

It is known that SFs in epitaxial layers can reach large sizes and they are classified as a separate group of epitaxial defects [39]. This is due to the peculiarity of epitaxial defects: being nucleated at the interface, they grow through the entire thickness of the epitaxial layer and come out on its surface. A characteristic feature of such SFs is not only the large size but also the single size of these defects for each type, which is determined by the thickness of the epitaxial layer.

The similarity of defect formation in diamond and silicon carbide is due to the high Debye temperature (it is 2230°K for diamond, and 1080°K for SiC) and the relatively low epitaxy temperature (950°C). Under these conditions and in the absence of inheritance from the substrate, defects such as dislocations are little active; they do not arise in the process of growth due to lack of energy. Much less energy is needed to form SFs, that is why these were the type of defects that became the main defects in the studied diamond plate. The study of SFs in diamond is yet to come.

We will focus on macrodefects in the following. Their discovery in diamond for the first time can change existing ideas about the structural features of almost perfect dislocation-free crystals. Defects of this type may not be a rarity, but a certain characteristic of the structure of almost perfect crystals, associated with large-scale (of the order of 1 mm and even larger) inhomogeneity in the distribution of microdefects. The reason for their rare observation is the infrequent use of the sectional XRT method in materials science, especially in the case of recording a series of sectional topograms covering a large volume of crystals, and they are not detected by other methods. We believe that such defects can only exist in dislocation-free crystals due to the fact that dislocations are active sinks for microdefects, preventing them from combining into clusters. Macrodefects are associated with very weak stresses in the crystal lattice. As can be seen from Figure 1, *b*, they have no effect on the broadening of the RC and most likely they have no a significant effect on the physical properties of the crystals.

5. Conclusion

It has been shown that, under certain conditions, the homoepitaxial growth of CVD-diamonds on a HPHT diamond substrate occurs without inheriting linear and planar defects of the substrate. Only the inheritance of strong local stresses associated with random inclusions and boundaries of growth sectors is possible. It has been established that the main defects in the grown crystal are bulk stacking faults of shape, structure, and size not previously observed in diamond. These defects coexist together with defect-free regions of the crystal and, when localized in a subsurface layer with a thickness of $20-30\,\mu$m, result in broadening of double-crystal RCs. The broadening of RC is noticeably affected by regions of strong local stresses inherited from the substrate. In defect-free regions, the structural perfection of CVD-diamonds is comparable to the quality of HPHT-grown crystals, making them suitable for the manufacture of X-ray optics elements.

For the first time, macrodefects were discovered in a diamond of high structural perfection in the absence of dislocations, previously observed only in dislocation-free silicon crystals.

Funding

The study was carried out with partial support of the State assignment of the Ioffe Physical-Technical Institute of Russian Academy of Sciences on the topic No. 0040-2019-0016, with partial support of the State assignment of the Valiev Institute of Physics and Technology of Russian Academy of Sciences on the topic No. FFNN-2022-0019. Part of the experimental study was carried out with the instrumental support of the „Research of Nanostructured, Carbon, and Superhard Materials“ Center for Shared Equipment of FSBI TISNCM.

Conflict of interest

The authors declare that they have no conflict of interest.

References

[1] R.S. Balmer, J.R. Brandon, S.L. Clewes, H.K. Dhillon, J.M. Dodson, I. Friel, P.N. Inglis, T.D. Madgwick, M.L. Markham, T.P. Mollart, N. Perkins, G.A. Scarsbrook, D.J. Twitchen, A.J. Whitehead, J.J. Wilman, S.M. Woollard. J. Phys.: Condens. Matter **21**, 364221 (2009). DOI: 10.1088/0953-8984/21/36/364221

[2] I. Nam, C.-K. Min, B. Oh, G. Kim, D. Na, Y.J. Suh, H. Yang, M.H. Cho, C. Kim, M.-J. Kim, C.H. Shim, J.H. Ko, H. Heo, J. Park, J. Kim, S. Park, G. Park, S. Kim, S.H. Chun, H. Hyun, J.H. Lee, K.S. Kim, I. Eom, S. Rah, D. Shu, K.-J. Kim, S. Terentyev, V. Blank, Y. Shvyd'ko, S.J. Lee, H.-S. Kang. Nature Photon. **15**, 435 (2021). DOI: 10.1038/s41566-021-00777-z

[3] C. Ponchut, J.M. Rigal, J. Clément, E. Papillon, A. Homs, S. Petitdemange. JINST **6**, C01069 (2011). DOI: 10.1088/1748-0221/6/01/C01069

[4] S. Pezzagna, J. Meijera. Appl. Phys. Rev. **8**, 011308 (2021). DOI: 10.1063/5.0007444

[5] H. Umezawa, M. Nagase, Y. Kato, S. Shikata. Diamond Rel. Mater. **24**, 201 (2012). DOI: 10.1016/j.diamond.2012.01.011

[6] J.J. Gracio, Q.H. Fan, J.C. Madaleno. J. Phys. D **43**, 374017 (2010). DOI: 10.1088/0022-3727/43/37/374017

[7] A.K. Mallik. J. Coat. Technol. Res. **3**, 75 (2016). DOI: 10.6000/2369-3355.2016.03.02.4

[8] R.C. Burns, A.I. Chumakov, S.H. Connell, D. Dube, H.P. Godfried, J.O. Hansen, J. Härtwig, J. Hoszowska, F. Masiello, L. Mkhonza, M. Rebak, A. Rommevaux, R. Setshedi, P. Van Vaerenbergh. J. Phys.: Condens. Matter **21**, 364224 (2009). DOI: 10.1088/0953-8984/21/36/364224
[9] Y. Shvyd'ko, S. Stoupin, V. Blank, S. Terentyev. Nature Photon. **5**, 539 (2011). DOI: 10.1038/nphoton.2011.197
[10] P.M. Martineau, M.P. Gaukroger, K.B. Guy, S.C. Lawson, D.J. Twitchen, I. Friel, J.O. Hansen, G.C. Summerton, T.P.G. Addison, R. Burns. J. Phys.: Condens. Matter **21**, 364205 (2009). DOI: 10.1088/0953-8984/21/36/364205
[11] A.B. Muchnikov, A.L. Vikharev, A.M. Gorbachev, D.B. Radishev, V.D. Blank, S.A. Terentiev. Diam. Rel. Mater. **19**, 432 (2010). DOI: 10.1016/j.diamond.2009.11.012
[12] H. Sumiya, K. Harano, K. Tamasaku. Diam. Rel. Mater. **58**, 221 (2015). DOI: 10.1016/j.diamond.2015.08.006
[13] M.A. Doronin, S.N. Polyakov, K.S. Kravchuk, S.P. Molchanov, A.A. Lomov, S.Yu. Troschiev, S.A. Terentiev. Diam. Rel. Mater. **87**, 149 (2018). DOI: 10.1016/j.diamond.2018.05.016.
[14] F.V. Kaminsky, O.D. Zakharchenko, R. Davies, W. Griffin, G.K. Khachatryan-Blinova, A. Shiryaev. Contrib. Mineral. Petrol. **140**, 734 (2001). DOI: 10.1007/s004100000221
[15] J. Walker. Rep. Prog. Phys. **42**, 1605 (1979). DOI: 10.1088/0034-4885/42/10/001
[16] Q. Liang, Y.F. Meng, C.S. Yan, S. Krasnicki, J. Lai, K. Hemawan, H. Shu, D. Popov, T. Yu, W. Yang, H.K. Mao, R.J. Hemley. J. Superhard Mater. **35**, 195 (2013). DOI: 10.3103/S1063457613040011
[17] A.R. Lang. J. Appl. Cryst. **27**, *6*, 988 (1994). DOI: 10.1107/s0021889894006734
[18] A.R. Lang, G. Pang, A.P. Makepeace. J. Synchrotron Rad. **3**, 163 (1996). DOI: 10.1107/S0909049596004268
[19] S. Shikata. Funct. Diam. **2**, *1*, 175 (2022). DOI: 10.1080/26941112.2022.2149279
[20] Y. Sato, K. Miyajima, S. Shikata. Diam. Rel. Mater. **126**, 109129 (2022). DOI: 10.1016/j.diamond.2022.109129
[21] M.P. Gaukroger, P.M. Martineau, M.J. Crowder, I. Friel, S.D. Williams, D.J. Twitchen. Diam. Rel. Mater. **17**, 262 (2008). DOI: 10.1016/j.diamond.2007.12.036
[22] I.A. Prokhorov, A.E. Voloshin, D.A. Romanov, A.P. Bolshakov, V.G. Ralchenko, Kristallografiya **64**, *3*, 369 (2019). (in Russian). DOI: 10.1134/S002347611903024X
[23] M. González-Mañas, B. Vallejo. J. Appl. Cryst. **51**, 1684 (2018). DOI: 10.1107/S1600576718015388
[24] W. Wierzchowski, M. Moore. Acta Cryst. A **51**, 831 (1995). DOI: 10.1107/S0108767395007690
[25] W. Kaiser, W.L. Bond. Phys. Rev. **115**, *4*, 857 (1959). DOI: 10.1103/PhysRev.115.857
[26] A.R. Lang. Proc. R. Soc. Lond. A DOI: 10.1098/rspa.1974.0150
[27] A.A. Shiryaev, D.A. Zolotov, O.M. Suprun, S.A. Ivakhnenko, A.A. Averin, A.V. Buzmakov, V.V. Lysakovskyi, I.G. Dyachkova, V.E. Asadchikov. Cryst. Eng. Commun. **20**, *47*, 7700 (2018). DOI: 10.1039/C8CE01499J
[28] S.N. Polyakov, A.A. Lomov, S.Yu. Martyushov, I.L. Shulpina, Yu.V. Shvydko, V.N. Denisov, N.V. Kornilov, V.D. Blank, Tez. dokl. KELT-2021, Chernogolovka (2021), S. 268. (in Russian).
[29] S.N. Polyakov, V.N. Denisov, A.A. Lomov, I.L. Shulpina, S.Yu. Martyushov, N.V. Kornilov, V.D. Blank. Phys. Status Solidi RRL **16**, *11*, 2200164 (2022). DOI: 10.1002/pssr.202200164
[30] B.K. Tanner, D.K. Bowen. Characterization of Crystal Growth Defects by *X*-Ray Methods. Plenum Press, N.Y. (1980). 589 p. DOI: 10.1007/978-1-4757-1126-4
[31] D.K. Bowen, B.K. Tanner, Vysokorazreshayuschaya rentgenovskaya difraktometriya i topografiya, Nauka, SPb (2002), 274 s. (in Russian).
[32] I.L. Shulpina, E.V. Suvorov, I.A. Smirnova, T.S. Argunova, ZhTF **92**, *10*, 1475 (2022). (in Russian). DOI: 10.21883/JTF.2022.10.53240.23-22.
[33] M.G. Milvidsky, Yu.A. Osipyan, E.V. Suvorov, I.A. Smirnova, E.V. Shulakov, Poverkhnost. Rentgenovskie, sinkhrotronnye i neytronnye issledovaniya **6**, 5 (2001). (in Russian).
[34] R.N. Kyutt, S.S. Ruvimov, I.L. Shulpina, Pisma v ZhTF **32**, *24*, 79 (2006). (in Russian).
[35] S.N. Polyakov, V.N. Denisov, N.V. Kuzmin, M.S. Kuznetsov, S.Yu. Martyushov, S.A. Nosukhin, S.A. Terentiev, V.D. Blank. Diam. Rel. Mater. **20**, 726 (2011). DOI: 10.1016/j.diamond.2011.03.012
[36] http://x-server.gmca.aps.anl.gov
[37] Z.G. Pinsker, Rentgenovskaya kristallooptika, Nauka, M., (1992), 391 s. (in Russian).
[38] E.N. Mokhov, I.L. Shul'pina, A.S. Tregubova, Yu.A. Vodakov. Cryst. Res. Technol. **16**, *8*, 879 (1981). DOI: 10.1002/crat.19810160804
[39] D.D. Avrov, A.O. Lebedev, Yu.M. Tairov, Izv. vuzov, Elektronika, **20**, *4*, 337 (2015). (in Russian).

Translated by Y.Alekseev